

Wind-induced seismic noise at the Princess Elisabeth Antarctica Station

Baptiste FRANKINET^{1,2}, Thomas LECOCQ¹, Thierry CAMELBEECK¹

¹Seismology-Gravimetry, Royal Observatory of Belgium, Brussels, Belgium

5 ²Glaciology Laboratory, Université Libre de Bruxelles, Brussels, Belgium

Correspondence to: Baptiste Frankinet (Baptiste.Frankinet@gmail.com)

Abstract. Icequakes are the result of processes occurring within the ice mass, or between the ice and its environment. Studying icequakes provides a unique view on ice dynamics, specifically on the basal conditions. Changes in conditions due to environmental, or climate, changes, are reflected in icequakes. Counting and characterizing icequakes is thus essential to monitor them. Most of the icequakes recorded by the seismic station at the Belgian Princess Elisabeth Antarctica Station (PE) have small amplitudes corresponding to maximal displacements of a few nanometres. Their detection threshold is highly variable because of the rapid and strong changes in the local seismic noise level. Therefore, we evaluated the influence of katabatic winds on the noise measured by the well-protected PE surface seismometer. Our purpose is to identify whether the lack of icequake detection during some periods could be associated with variations in the processes generating them or simply to a stronger seismic noise linked to stronger wind conditions. We observed that the wind mainly influences seismic noise at frequencies greater than 1 Hz. The seismic noise power exhibits a bilinear correlation with the wind velocity, with two different slopes at wind velocity lower and greater than 6 m/s, with, for example at a period of 0.26 s, a respective variation of 0.4 dB/(m/s) and 1.4 dB/(m/s). These results allowed presenting synthetic frequency and wind-speed dependent noise model that explain the behaviour of the wind-induced seismic noise at PE, which exhibits that seismic noise amplitude increases exponentially with increasing wind speed. This model enables us studying the influence of the wind on the original seismic dataset, which improves the observation of cryoseismic activity near the PE station.

1 Introduction: Icequakes

The study of icequakes provides insights into the different processes linked to ice dynamics. Icequakes, or cryoseisms, originate from the formation of crevasses, basal sliding, hydrofracturing, iceberg calving, englacial fracturing, and glacial seismicity triggered by an earthquake. A synthesis of the main types of icequakes and their causes is presented by Podolskiy & Walter (2016). Cryoseismic sources can have seismic signatures difficult to distinguish one from another. For example, the crevasse formation represents very short events (< 1 s) over a large frequency band (10 - 50 Hz). Crevasse formation events have a propagation velocity of 0.01 m/s up to 30 m/s and generally do not exceed 10 μ m in amplitude

(Podolskiy & Walter, 2016), making them close in amplitude to microseismic noise or to wind-induced ground motion that can cause similar seismic signature and amplitude (Bormann & Wielandt, 2013; Naderyan et al., 2016; Withers et al., 1996). Cryoseismology has not been studied thoroughly in all regions of Antarctica but thanks to the improvement of instrumentation and the increasing number of seismic stations in Antarctica, numerous studies linking seismology to glaciology have been published in the last decade. From linking the microseismicity induced by tides in the grounding line of East-Antarctica (Barruol et al., 2013), focusing on tremors from stick-slip motions in the Whillans ice stream (Winberry et al., 2013), studying specific cryoseismic events observed at Ekström Ice Shelf, Antarctica (Hammer et al., 2015), to observing thermally-induced icequakes and their origins on blue ice in East-Antarctica (Lombardi et al., 2019).

1.1 The Antarctica Princess Elisabeth Belgian station and seismic stations

The Belgian Princess Elisabeth Antarctica Station (PEAS) was built during the first International Polar Year 2007-2008 and completed in 2008-2009. It is situated 300 m North of Usteinen nunatak (71°57' S, 23°20' E) on a small flat granite ridge, a few kilometres north of the Sør Rondane mountain range. The Usteinen nunatak is approximately 700 m long and 20-30 m wide and is composed of massive coarse-grained granite with minor xenolithic blocks of metamorphic rocks (Kojima & Shiraishi, 1986). To the south, the Sør Rondane Mountains peaks have an elevation up to 4000 m and form part of the Eastern Antarctica Precambrian shield (Pattyn et al., 1992). The PEAS allowed investigation in the field of meteorites as spotting them on the emptiness of Antarctica is simpler than mixed up with vegetation and rocks, to microbiology (Peeters et al., 2011; Pushkareva et al., 2018), glaciology (Callens et al., 2015; Pattyn et al., 2010), and meteorology (clouds, aerosols, temperature) (Gossart et al., 2019; Gossart et al., 2019; Herenz et al., 2019; Souverijns et al., 2018). In parallel, the Royal Observatory of Belgium installed a permanent broadband seismic station (BE.ELIS) on the bedrock near the base in February 2012 (Camelbeek et al., 2019). This station increases the sparse coverage of seismic stations in the Sør Rondane mountain range in Antarctica. Indeed, the closest seismometer is located at the Russian Novolazarevskaya base, 430 km West of PEAS. To the East of PEAS, the closest station is the Japanese Syowa site (680 km away). Because of its location, the station gave a new source of information for global seismic studies as well as for inferring the crustal structure beneath it (Camelbeek et al., 2019). The addition of a temporary seismic network during the 2014 austral summer (see Table 1 and Figure 1) has highlighted seismic activity, within a radius of 150 km around the station (Camelbeek et al., 2019). This seismic activity is related to the interaction between ice and bedrock or from within the ice.

1.2 Icequakes and seismic noise

Most icequakes induce elastic deformation which can be detected by seismometers while the resulting plastic damage and movements of the ice sheet and associated glaciers can be observed by other geophysical or geodetic means, such as GPS (Capra et al., 1998) or radar interferometry (Mohr et al., 1998; Rignot et al., 2011). Cryoseismic catalogues and seismic observations can be correlated with numerical models of eastern Antarctic ice dynamics to constrain subglacial properties of a specific area (Lipovsky & Dunham, 2015; F. Pattyn, 2010; Smith, 1997, 2006). These icequakes mostly have

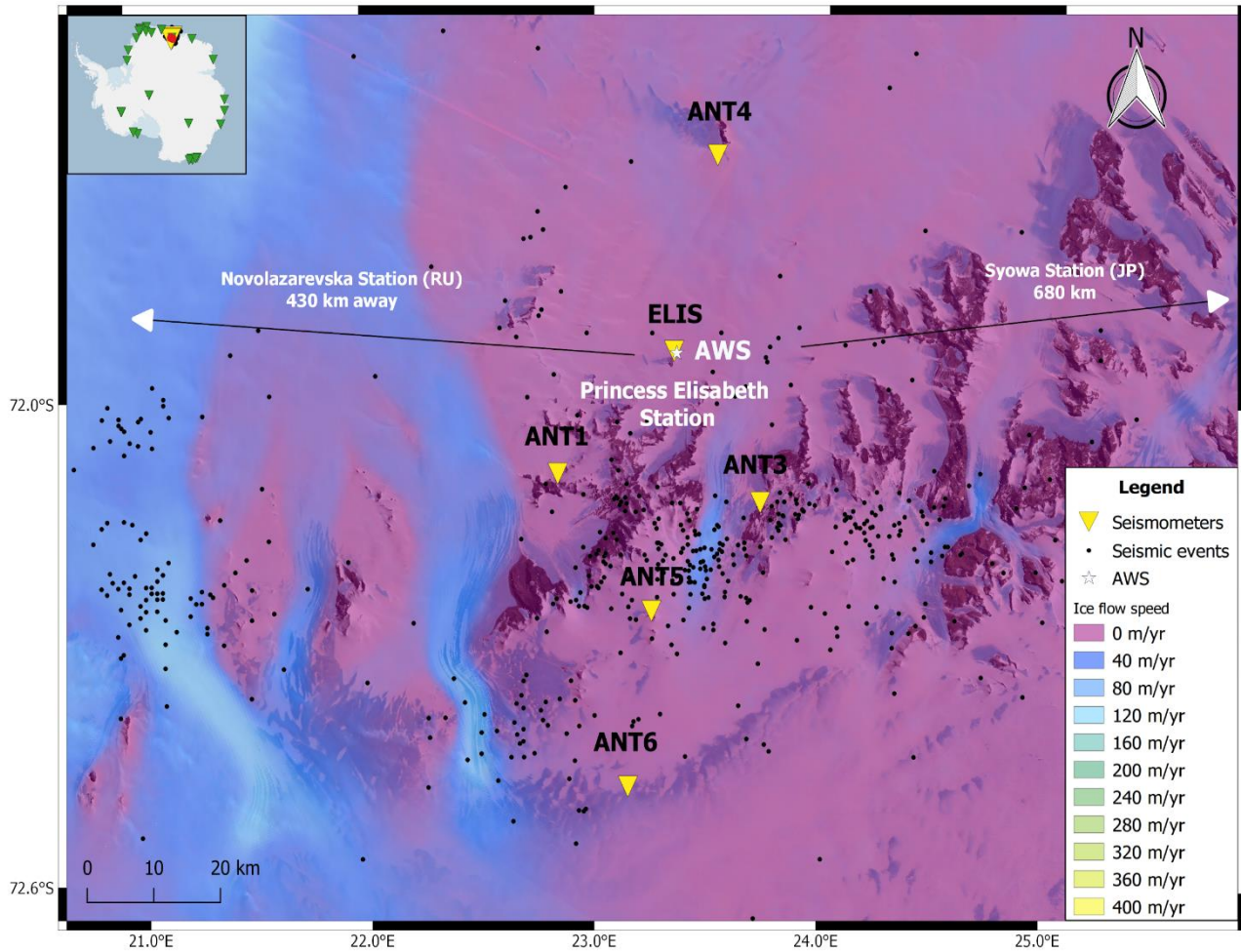
a very low seismic amplitude (few nanometres of displacement) but can still be detected owing to the very low seismic noise observed in Antarctica. Icequakes' signal-to-noise ratios (SNR) decrease when the noise increases, hence it is important to identify the noise sources and their power to impact the catalogue completeness before concluding the ice dynamics. At PEAS, a few anthropogenic noise sources exist year-round like wind turbines, and seasonal human activities outside and inside the buildings during the summer. The region is also subjected to rough meteorological conditions, composed of katabatic winds with sometimes velocities higher than 25 m/s (Pattyn et al., 2010). Such high-velocity winds have been known to affect the seismic data (Johnson et al., 2019; Lott et al., 2017) because the kinetic energy in the wind is converted to mechanical energy on reaching the instrument enclosure, thus contributing noise to the seismic record (Walker & Hedlin, 2010). This wind-induced seismic noise depends on wind velocity (Johnson et al., 2019). Understanding the effect of wind-induced seismic noise is crucial in monitoring icequakes and to understand its potential to obscure icequakes.

The PEAS and its permanent seismometer (ELIS) are relatively well protected from the strongest katabatic winds from the Antarctic plateau by a mountain range. ELIS is located on the same flat granite ridge as the Princess Elisabeth Station and inside a shelter, 350 m from the base. Compared to ELIS, the temporary seismometers installed in 2014 (Figure 1) are less protected, and more prone to wind noise. If ELIS sees an increase of seismic amplitude related to wind, the temporary seismic stations should therefore have an increased wind-induced ground motion. The base is powered by solar panels and nine Proven Energy 6kW wind turbines (WT) (Belspo, 2007). Each consists of a 9 m high tower with a 3-blade rotor that adapts the angle of the blades with the wind speed to generate the maximum amount of power from low-velocity winds and reduce the amount from high-speed winds. When the wind speed is low, the angle of the three blades is reduced up to 5° and when the wind speed is the highest, the angle can increase up to 45° which reduces by half the 5.5 m rotor diameter and the resulting rotational speed. The effect of wind turbines on seismic records has also been studied in the past and often results in noise increases in discrete frequency bands related to their shape, structure, height, the number of blades, and rotational speed (Mucciarelli et al., 2005; Stammler & Ceranna, 2016; Withers et al., 1996). Wind-induced seismic energy has a wide range of frequencies (1 - 60 Hz and below 0.05 Hz), and its amplitude decreases rapidly with depth (Withers et al., 1996). Wind-induced seismic noise characteristic frequencies and amplitudes also depend on wind interaction with man-made constructions (Hillers et al., 2015; Johnson et al., 2019; McNamara, 2004; Stammler & Ceranna, 2016). In Antarctica, given the lack of trees, the seismic noise induced by the wind should likely originate from the interaction with the base's buildings, wind turbines, and topography.

In this paper, we present an analysis of the influence of the wind velocity onto the seismic data from the ELIS seismometer at the Princess Elisabeth Station. As reported in Johnson et al. (2019) and Lepore et al. (2016), by sorting seismic data for different wind speeds, we quantify the relationship between wind energy and seismic ground motions. We present a model of the noise baseline when there is no wind and its increase for each increment of wind speed, in all frequency bands. Using this model, we compute a model of the wind-induced seismic noise for ELIS. We applied a similar model to each station of the temporary seismic network (ANT). Finally, we used these models to evaluate the impact of the wind noise on the detectability of icequakes

Our dataset includes seismic and wind velocity measurements at the PEAS base and seismic signals recorded between January and April 2014 by five temporary seismic stations, the ANT network, installed in the Sør Rondane Mountains (Figure 1). The seismic data at the PEAS comes from the broadband seismic station (ELIS) installed in February 2012 (Camelbeeck et al., 2019; Lombardi et al., 2019). This station worked irregularly up to the end of 2016 due to
100 difficulties providing continuous power supply during the austral winter, but recordings are continuous for the years 2017, 2018, 2019, 2020. The data collected by the ANT stations concern the period from January – April 2014. ELIS as well as the other temporary stations except for ANT4 use Trillium 120P, 120 s seismometers that sample at 100 Hz, giving a recording bandwidth from 0.008 to 50 Hz, allowing to record small local seismic events as well as the teleseismic earthquakes (Camelbeeck et al., 2019). ANT4 is a Streckeisen STS-2 gen3 120 s seismometer (see Table 1).

105 The wind data comes from an Automated Weather Station (AWS) designed by the Institute for Marine and Atmospheric Research, Utrecht University (UU/IMAU) (van den Broeke, 2006) and is provided by the AEROCLOUD project (<http://ees.kuleuven.be/hydrant/aerocloud/>) (Gorodetskaya et al., 2010). The AWS is installed 300 m from the Princess Elisabeth Station, close to the ELIS seismometer site (see Figure 1 and Table 1). It has been working since February 2009 and was replaced by a new AWS in December 2015, which is still in operation. The AWS is designed to work for long
110 periods without being serviced and offers the opportunity to measure meteorological variables in remote areas and harsh weather conditions. These stations register wind speed, direction, temperature, humidity, atmospheric pressure at 2.0 m above the ground surface, averaged over an hour window. The AWS records wind speeds from 0 to 60 m/s (+/- 0.3 m/s) and 0 to 360° direction (+/- 3°). We use the seismic data from the ELIS station for the period 01 January 2017 - 31 December 2017, to extract hourly Power Spectral Density (PSD), which describes the seismic power in the signal as a function of
115 frequency. Probabilistic PSD represents a statistical distribution of the PSDs (McNamara, 2004). PSDs are computed using the Obspy package (Beyreuther et al., 2010) based on the McNamara method (McNamara, 2004) which estimates the PSD via a finite-range Fast Fourier Transform (FFT) of the original data (see parameters in Appendices). The ground motion time series are corrected for the instrument response and calculated to PSDs in decibels [dB (m/s²)²/Hz] to allow the comparison with the new high/low Peterson noise models (Peterson, 1993). We apply the same processing to compute the hourly PSDs
120 for the five stations of the ANT network. We compute PSDs for every hour-segment of the entire year, to match the time step of the wind data of the AWS station. The PSD is calculated with a low smoothing of 1/40th of an octave at each central frequency/period. This is important to allow identifying characteristics buried in the noise such as weak narrow seismic peaks. Due to the sampling rate of the ANT network (100 Hz), we limited our computations to 50 Hz: the Nyquist frequency.



125 **Figure 1: Network of instruments used in this study: 1 permanent (ELIS) and 5 temporary (ANT-) seismic stations. Other seismic**
stations in Antarctica reported by the International Seismograph Station Registry (<http://www.isc.ac.uk/registries>) are shown on
the context map (green triangles) and the 2 closest from Princess Elisabeth Station are pointed towards with a white arrow: Novo.
(RU) and Syowa (JP). The cryoseismic activity (Camelbeeck et al., 2019) registered by a minimum of 4 stations during the working
time of the ANT network (January - May 2014) is shown by the small dark dots (Ice flow speed from Mouginit et al., 2019).

130

135

Station	Instrument	Location	Latitude [°]	Longitude [°]	Elevation [m]	Start	End
ELIB	Nanometric s Trillium 120P, 120 s	Princess Elisabeth Antarctica Station (borehole)	-71.947	23.346	1359	2010-02-15	2014-06-13
ELIS	Trillium 120P, 120 s	Princess Elisabeth Antarctica Station (surface)	-71.947	23.347	1372	2012-02-11	In service
ANT1	Trillium 120P, 120 s	Otto	-72.099	22.840	1718	2014-01-02	2014-04-14
ANT3	Trillium 120P, 120 s	Gunnestadbree n (outlet glacier)	-72.134	23.727	1397	2014-01-04	2014-04-14
ANT4	Streckeisen STS-2 gen3	Vesthaugen hill (west hill)	-71.703	23.529	1217	2014-01-25	2014-08-25
ANT5	Trillium 120P, 120 s	Last Nunatak	-72.271	23.252	2366	2014-01-07	2014-03-31
ANT6	Trillium 120P, 120 s	Blue-Ice	-72.488	23.150	2379	2014-01-07	2014-12-05
AWS	Young 05103	Princess Elisabeth Antarctica Station	-71.949	23.358	1420	2009-02-02	In service

Table 1: Belgian Antarctica Seismometers information and Automatic Weather Station (AWS) information from the AEROCLOUD Project.

3.1 Wind Induced Noise Model for ELIS

To quantify the link between wind velocity and seismic noise at the PEAS base, we computed hourly PSDs of the ELIS vertical seismometer for the whole year 2017 extracting the 5th percentile amplitude for every 0.25 m/s wide bin of wind speed between 0 and 25 m/s (Figure 2). The wind speed used in this study is the 1-hour average of the maximum wind speed recorded by the AWS every 10 minutes. The 5th percentile is preferred over the average to define base noise levels for each wind speed step without taking outliers into account. The wind speed steps and their base noise amplitude exhibit (Figure 2) an increase of noise amplitude at all periods, but the effect is stronger below 2 s and above 10 s.

The seismic noise levels increase with the wind velocity and exhibit two different behaviours for wind velocity greater and smaller than 6 m/s. The increase of seismic noise is moderate for wind velocity from 0 to 6 m/s and larger above 6 m/s. At 0.1 s (10 Hz) there is a 42 dB difference between 0 and 25 m/s, which corresponds to a ground acceleration increase of 100 times. The wind-noise effect is higher on the horizontal components than on the vertical component of the seismometer. This has been already observed and is due to the direct interaction of the wind travelling horizontally inducing tilt noise on the seismometer (Mucciarelli et al., 2005). To create the synthetic noise model, we need to quantify seismic noise changes at each frequency with respect to the wind speed amplitude. For each period band, two linear relationships are determined between 0 and 6 m/s and above 6 m/s (slopes a_1 and a_2 in Figure 3a), explained by Equation (1). Although the two linear regressions are computed independently, they do predict very similar values for 6 m/s at all periods (difference lower than 0.01 dB), making the bilinear relationship continuous.

$$f(x) = \begin{cases} a_1x + b_1, & \text{if } 0 < x \leq 6 \quad (1) \\ a_2x + b_2, & \text{if } x \geq 6 \quad (2) \end{cases} \quad (1)$$

Equation (1) describes the bilinear relationship $f(x)$ predicting the amplitude in dB $(\text{m/s}^2)^2/\text{Hz}$ using x , the wind speed in m/s; and the slope and intercept parameters a_1 , a_2 and b_1 , b_2 obtained from the linear regressions.

The data used for the weighted regression is the 5th percentile of wind speeds binned by 0.25 m/s with a minimum of 10 observations per bin. The weights are defined as the inverse of the standard deviation within each bin. For example, Figure 3b shows the two linear regressions at the 0.26 s period (dashed vertical line on Figure 3a): the wind-induced noise increases by approximately 2 dB from 0 to 6 m/s, and after 6 dB it increases by 1.5 dB/m/s. The lower number of occurrences of wind speeds above 10 m/s could lead to instability of the regression, but between 6 and 10 m/s it is robust and fits the observations at higher wind speed. The linear regressions are computed for every frequency and therefore describe the behaviour of the seismic noise induced by the wind at ELIS.

Once the linear parameters are determined for each period of the spectrum, using Equation (1), we can run the model for any theoretical wind speed to obtain a synthetic PSD spectrum. For different wind speeds, we generate a synthetic frequency and wind-speed dependent noise model (Figure 4a). Transforming the synthetic PSDs to ground velocity amplitude requires

175 integration to PSDs of velocity and the application of Parseval's theorem that links the power spectrum and the RMS (root mean square) of a signal. The RMS velocity calculated in the 1-50 Hz frequency band (Figure 4b), i.e. the band where most cryoseismicity is expected to occur, shows an exponential increase from 0.2 to 2.8 $\mu\text{m/s}$ between 0 and 25 m/s wind speed. Figure 4b also shows the frequency band (8-50 Hz) and the RMS amplitudes (smaller than 0.3 $\mu\text{m/s}$) of the icequakes signals studied by Lombardi et al. (2019). This illustrates that, based on our model, Lombardi et al. (2019) are vulnerable to missing seismic events when the wind speed exceeds 10 m/s.

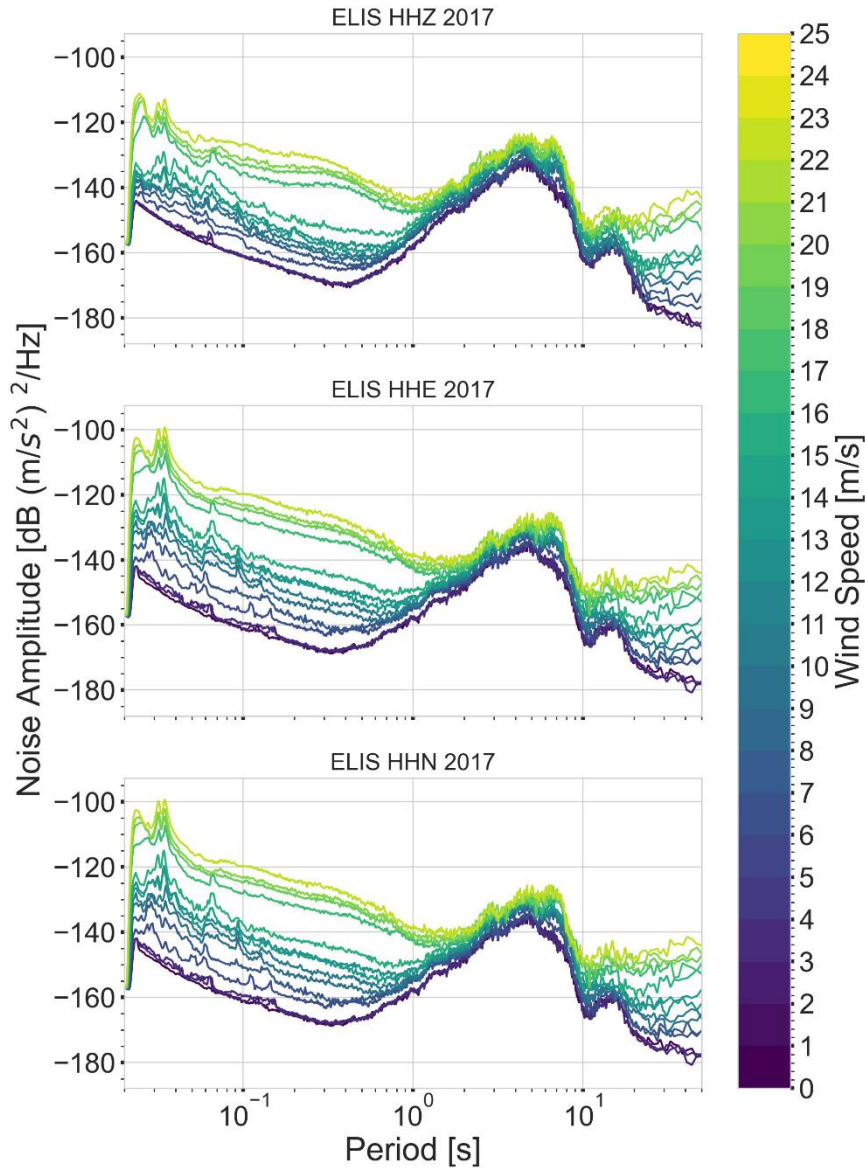
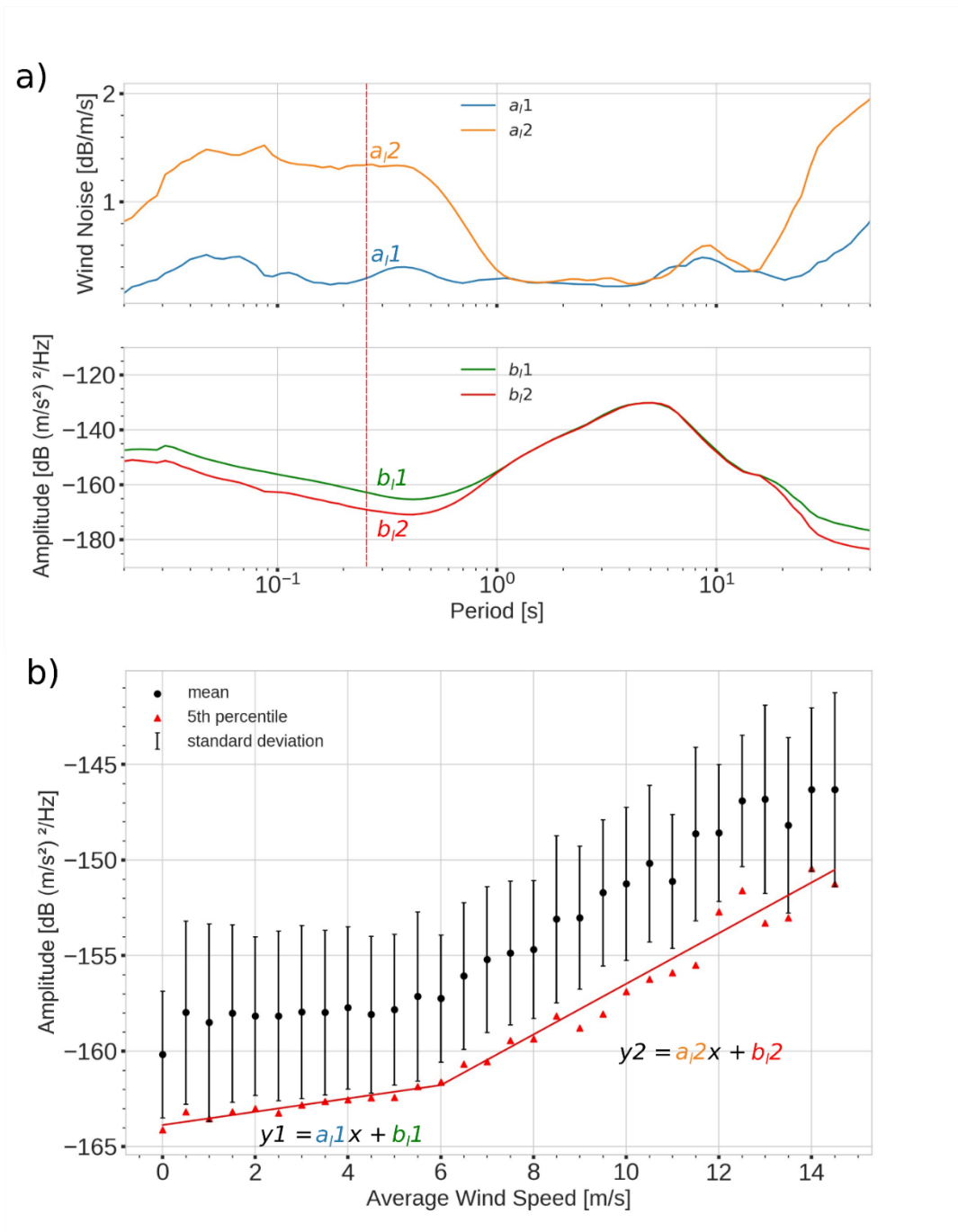


Figure 2: 2017 ELIS PSDs computed for 0 – 25 m/s wind speed. HHZ, HHE and HHN are the vertical, East-West, and North-South channels, respectively.



180

Figure 3: a): Wind Induced Noise Model describing the parameters of 2 linear functions for every period of ELIS HHZ in 2017: The first subplot represents the “a” parameter in the linear regression $y = ax + b$ and the second shows the “b” parameter. Those 2 different linear relation parameters are until 6 m/s ($a_{i,1}/b_{i,1}$) and after 6 m/s ($a_{i,2}/b_{i,2}$). b): Behaviour of the 5th percentile (red) and mean (black) noise amplitude vs the average wind speed [m/s] for the 0.26 s period (red dotted line on figure 3 a) There are 2 different red linear functions: before 6 m/s ($y1$) and after 6 m/s ($y2$).

185

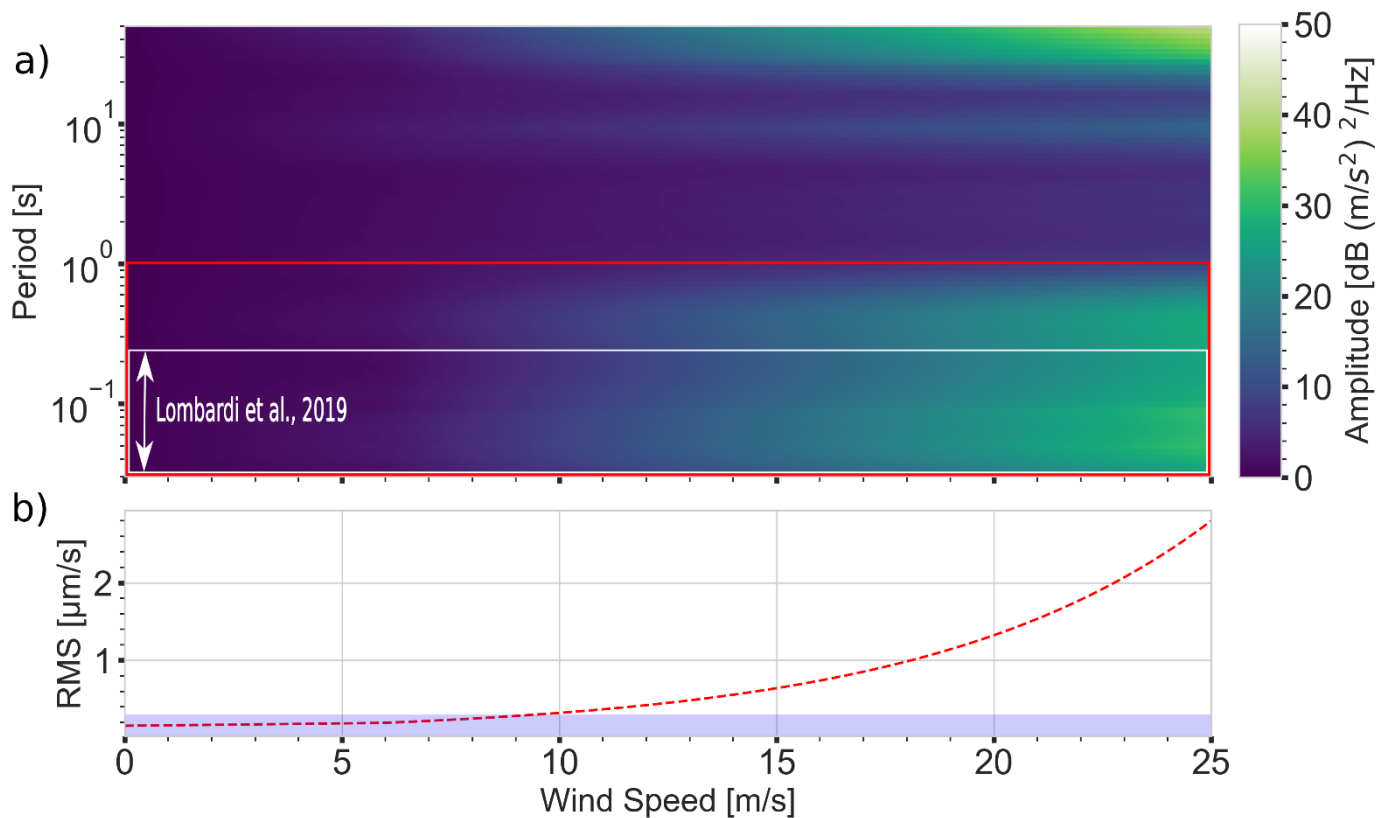


Figure 4: a) Synthetic frequency and wind-speed dependent noise model representing wind-induced noise increase; in white is the frequency range of the thermally-induced icequakes observed by Lombardi et al., 2019. b) The 1 – 50 Hz RMS ground speed at ELIS HHZ extracted from the red rectangle on subplot a) and in light blue the amplitude range of these icequakes.

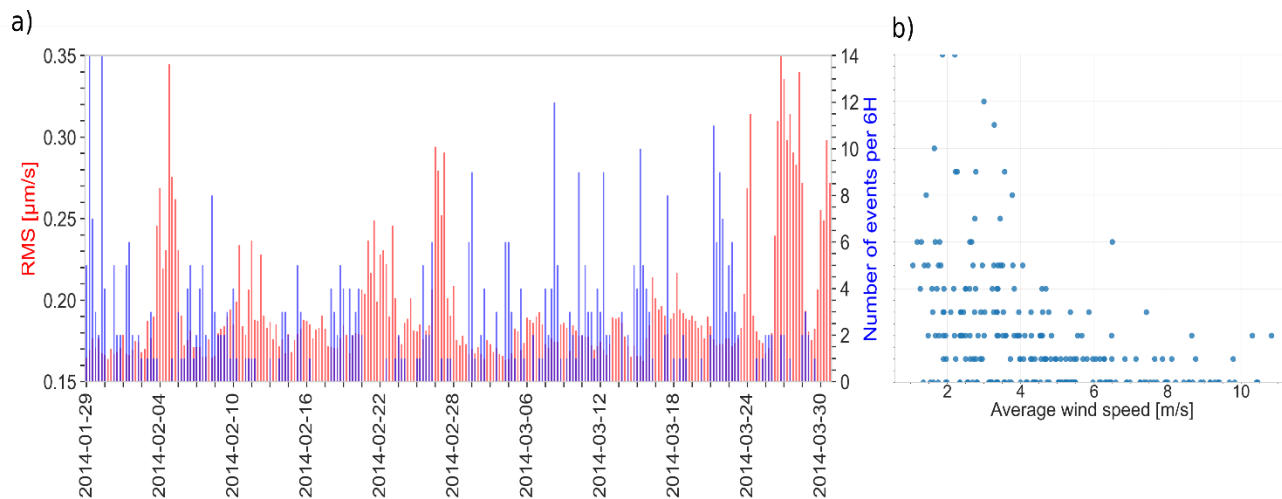


Figure 5: a) RMS per 6h calculated from the average wind speed and the noise model seen at ELIS vs the icequake rate per 6h (seismic rate) by Camelbeck et al. (2019). b) Icequake rate per 6h vs Average wind speed [m/s]

3.2 Seismic Noise for the ANT network

We used our model to evaluate the completeness of the catalogue of icequakes identified between January and April 2014 by the ANT temporary seismic network, including the ELIS station. The icequake rate detected per 6 hours, located by Camelbeeck et al. (2019), shows an inverse correlation with the seismic noise level deduced by our model (RMS) from the wind speed measured at PEAS (Figure 5). This RMS is calculated from the mean wind speed registered by the AWS averaged per 6h using our model shown in Figure 4b. This inverse correlation suggests that the variation in the icequake rate would be directly related to seismic noise conditions induced by the wind. For example, from the 3rd to the 4th of February 2014 (A), the RMS increase from 0.17 to 0.35 $\mu\text{m/s}$ at the maximum peak. Over the period presented in Figure 5 (29th January 2014 – 30th March 2014), 472 events were detected by Lombardi et al. (2019). If these events were equally distributed over the time period, ~ 7.9 events could be detected each day but, the numbers of events found over this period were not, as for example, during the 3rd of February 5 events were detected whereas, on the 4th of February, not a single event was recorded which could be a result of the drastic RMS increase.

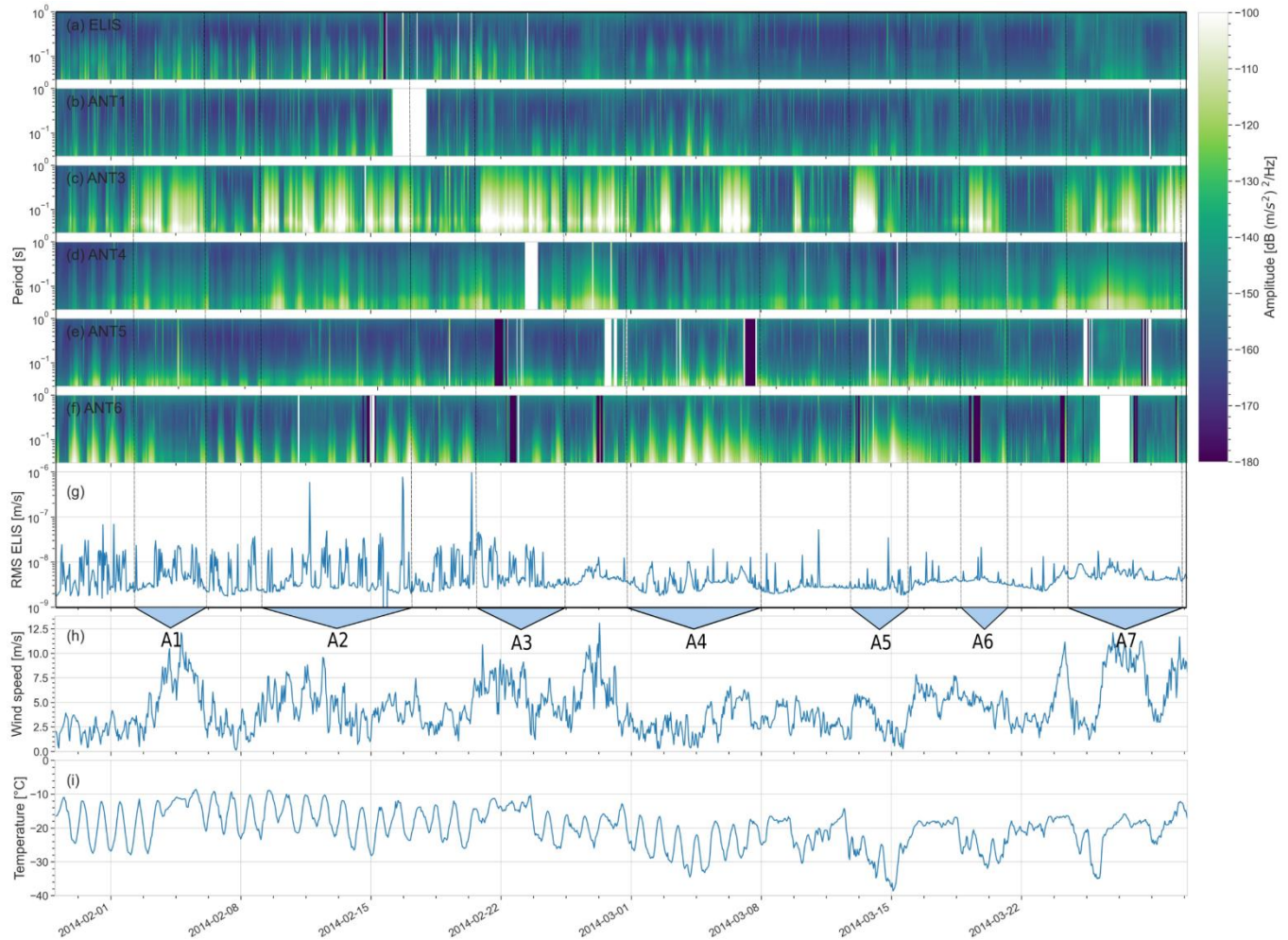
ELIS is located in an area where the ice sheet moves very slowly. Therefore, the ice sheet movements did not contribute greatly to the recorded seismic noise level at the ELIS seismic station. Using the 2014 data from the AWS, we could compute a synthetic noise amplitude for the wind-generated noise during the deployment of the temporary ANT network. In the case of the wind field and its effects on ELIS would be identical at the other seismometers, we could obtain “clean” spectrograms by withdrawing the frequency-dependent noise increase due to wind. Because of the large dimension and different geographical contexts of each station, this assumption might not necessarily hold. Figure 6a-f shows the spectrograms for the 6 stations, which highlight the contribution of the cryoseismic activity of the East-Antarctic ice-sheet and potentially wind-generated noise in the seismic data of each station. Figure 6g-l represents the RMS velocity of the ELIS station. For comparison, the average wind speed and temperature recorded at ELIS (Figure 6h-i) are shown.

The periods where the RMS velocity of the stations shows a significant cryoseismic activity are indicated by blue arrows labelled A1 to A7 (Figure 6l). Some stations, and particularly ANT3 and ANT6, do also exhibit a correlation between the increase of wind speed and their recorded noise amplitude.

Between the 8 - 20 January (A1), there is a small co-increase of wind speed and noise amplitude, especially at ANT3. The same thing happens during the 8 - 15 February (A2) and 20 - 26 February (A3) intervals. 1 - 7 March (A4) shows noise amplitude peaks for all stations but ELIS, ANT1, and ANT4. The 13 - 15 March (A5) starts with a strong activity at ANT3 and then an increase in the other stations, including strong peaks at ANT6. The 18 - 20 March period (A6) has more energy on ANT3 than the other stations. The 23 - 27 February period (A7) is again dominated by strong energy at ANT3 but other stations peak during that period too (ANT6 and ANT1 particularly). The activity of ANT3 seems, in general, to be higher than on the other stations, between 1 - 28 February and after 15 March (end of A5) until the rest of the deployment.

In addition to the activity spanning over several days, the six stations show a strong diurnal activity which was shown to be linked to temperature variation that induces thermally-induced icequakes (Lombardi et al., 2019). Its intensity is larger at

ANT6 throughout the deployment period. At all stations but especially at ELIS and ANT1, the diurnal effect seems to lessen after 8 March 2014 (A4).



230 **Figure 6: Belgian Antarctica Network Spectrograms (1 – 50 Hz) without wind noise for the 29/01/2014 – 30/03/2014 period with the RMS for ELIS and the average wind speed [m/s] and temperature [°C] for the same period from the AWS station at ELIS. A1 – A7 represent periods of increased amplitude.**

4 Discussion

The origin of the diurnal activity could come from thermally-induced icequakes resulting from diurnal temperature differences as observed and studied at ELIS (Lombardi et al., 2019; Winter et al., 2021). On all stations but especially at
 235 ANT5 and ANT6, there is a greater diurnal activity during A4 and A5, which correlates from a sudden drop of temperature and a greater temperature difference of 10°C between the daytime/nighttime (Figure 6). This also suggests that part of the greater activity seen at ANT3 and ANT4 is most likely caused by a greater cryoseismic activity induced by the temperature

change between the daytime/nighttime. During A6 and A7, the same effect is observed, and the activity greatly increased at ANT3 together with temperature deltas of about 10°C. The stronger diurnal activity at ANT6 can be explained by its setting: it is placed on blue ice and is, therefore, better coupled to register crevassing and thermally-induced icequakes than the other stations on rock (Trnkoczy et al., 2012). This diurnal activity at ANT5 has a higher frequency than the other stations and most of its energy release is above 30 Hz.

The ANT3 station has a much higher amplitude of seismic noise than any other station from the network. The activity at ANT3 seems to correlate with the wind for at least A1, A2, A3, and A7 periods. This indicates that to a certain extent the wind field at this station could be the same as at ELIS but that the wind strength and/or its effect on the seismic noise is greater. Nevertheless, certain peaks have a high amplitude that seems hard to link to the wind activity, at least not the same wind as the one measured in ELIS. For example, using our model, to reach the peaks at 1.0 $\mu\text{m/s}$ seen at ANT3, in A2, A3, and A4, the local wind speed needs to reach at least 17.5 m/s, which was not observed at ELIS during the period where the ANT network was deployed. The maximum wind speed during that period was 14 m/s. Another cause of the difference in energy could be linked to the insulation or coupling difference of the seismometer in the different stations. In the case of ANT3, part of the explanation for site-specific winds could come from its location close to an outlet glacier, which could channelize the winds originating from the Plateau to the south.

The continuously higher energy at ANT4 follows the same general long-term trends as the wind speed. This could be caused either by slightly stronger local winds, or a slightly steeper relationship between wind and noise caused by coupling or installation settings. Stronger continuous cryoseismic activity could also explain the observations: however, according to Lombardi et al. (2019) we would expect to see more diurnal variation if that activity is thermally induced. From the stations in the network, ANT1, ANT3, and ANT5 are the closest to the two most seismogenic zones, i.e: the collision zone between the glaciers and the mountains; and the channelized glaciers with greater ice flow speed (Figure 1).

In agreement to Lott et al. (2017) and their wind-induced noise study in the Dead Sea Valley, our results at PEAS show similar traits such as a linear increase of PSD in dB with wind speed that affects all observed frequencies (1 to 50 Hz). At PEAS and in the Dead Sea Valley, wind speeds as low as 5 m/s affect the detection of small seismic events due to increased noise levels by about 5 dB. The effect of wind speed is negligible in the microseism band, at frequencies between 0.1 and 1 Hz (Figure 3a), as also observed in the Dead Sea Valley, it is therefore likely that microseism monitoring is not adversely impacted by this noise which is encouraging for microseism noise-based imaging or monitoring of the area.

265 **5 Conclusions**

Near the Princess Elisabeth Station, we observe wind-induced seismic noise that in some cases prevents the detection of icequakes. The detection of icequakes can be adversely impacted by wind speed as low as 5 m/s, as they will be hidden in the wind-induced noise. When these winds reach their highest speeds, of up to 25 m/s, the seismometer registers an increase of 15 times the ground velocity of a stand-still moment (0.2 $\mu\text{m/s}$ to 3 $\mu\text{m/s}$) making most of the small icequakes

270 undetectable. Understanding the effect of wind-induced seismic noise is therefore crucial in monitoring icequakes as well as
understanding missing icequakes in the data. To mitigate wind-induced noise and improve the quality and detectability of
icequakes, we suggest, whenever possible, preferentially installing seismometers into boreholes, far from structures that
could be affected by wind, in a wind-protected area. In all cases, we recommend installing a meteorological station next to
each instrument site to obtain local measurements of the fields.

275 Using the data from the permanent seismic station ELIS, we provide a synthetic model that simulates the ground
motion spectrum for different wind speeds. For half of the period during which the temporary ANT network was deployed,
the ANT3 seismometer exhibits greater amplitude than the other stations which can only be partially explained by greater
local wind speeds. We found that seismic noise levels at different stations is mostly independent of the wind speed and
probably related to local icequake activity.

280 As observed elsewhere, we suggest that the diurnal changes of energy observed are linked to cycles of cryoseismic activity
induced by the large diurnal temperature delta. If the icequakes were very shallow events due to thermal expansion of ice,
then those are maybe not relevant for, e.g., basal processes, but nonetheless inform a diurnal ice process. The longer-lasting
energy releases, on the other hand, could have different causes related or not to wind. They could either originate from
different wind fields, wind speeds, or couplings; or from an increased cryoseismic activity occurring in the vicinity of the
285 station, independently from the diurnal and thermal effects, for example, crevasses or basal stick-slip events. The diurnal
seismic energy at a higher frequency on ANT5 could result from different source mechanisms, with smaller, shorter
icequakes occurring in the direct vicinity of the station. This could be confirmed by comparing the icequake signatures at the
different stations in future work.

Acknowledgements

290 We acknowledge the AEROCLOUD project (<https://ees.kuleuven.be/hydrant/aerocloud/>) for providing the wind data from
the Automated Weather Station (AWS) located at the Princess Elisabeth Station in Antarctica. The seismic data from the
permanent ELIS station as well as from the ANT array should be made available via the ORFEUS data centre soon, but in
the meantime, access can be given directly from the ROB FDSN web services. Baptiste Frankinet acknowledges the
financial support from the ROB.

295 We also acknowledge the ETH-Zurich that owns the ANT4 Streckeisen STS-2 gen3 120 s seismometer.
We thank QGIS and the Quantarctica module (Matsuoka et al., 2013) with which we drew the Figure 1 map.

300

References

- Barruol, G., Cordier, E., Bascou, J., Fontaine, F. R., Legrésy, B., & Lescarmontier, L.: Tide-induced microseismicity in the Mertz glacier grounding area, East Antarctica: MERTZ GLACIER TIDE-MODULATED ICEQUAKES. *Geophysical Research Letters*, 40(20), 5412–5416, <https://doi.org/10.1002/2013GL057814>, 2013.
- 305
- Belspo. Construction and operation of the new Belgian Research Station, Dronning Maud Land, Antarctica: Final Comprehensive Environmental Evaluation Report (CEE), Belgium, March 2007.
- Beyreuther, M., Barsch, R., Krischer, L., Megies, T., Behr, Y., & Wassermann, J.: ObsPy: A Python Toolbox for Seismology. *Seismological Research Letters*, 81(3), 530–533, <https://doi.org/10.1785/gssrl.81.3.530>, 2010.
- 310
- Bormann, P., & Wielandt, E.. Seismic Signals and Noise. *New Manual of Seismological Observatory Practice 2 (NMSOP2)*, 62, 2013.
- van den Broeke, Prof. M. R.: Automatic weather stations in interior East Antarctica, 2006.
- Callens, D., Thonnard, N., Lenaerts, J. T. M., Van Wessem, J. M., Van de Berg, W. J., Matsuoka, K., & Pattyn, F.: Mass balance of the Sør Rondane glacial system, East Antarctica. *Annals of Glaciology*, 56(70), 63–69, <https://doi.org/10.3189/2015AoG70A010>, 2015.
- 315
- Camelbeek, T., Lombardi, D., Collin, F., Rapagnani, G., Martin, H., & Lecocq, T. : Contribution of the seismic monitoring at the Belgian Princess Elisabeth base to East Antarctica ice sheet dynamics and global seismicity studies. *Bulletin Des Séances- Académie Royale Des Sciences d'outre-Mer*, 63, 2019.
- Capra, A., Frezzotti, M., Mancini, F., Radicioni, F., & Vittuari, L. : GPS for ice sheet movement monitoring and grounding line detection. In R. Forsberg, M. Feissel, & R. Dietrich (Eds.), *Geodesy on the Move* (Vol. 119, pp. 486–491). Berlin, Heidelberg: Springer Berlin Heidelberg, https://doi.org/10.1007/978-3-642-72245-5_82, 1998.
- 320
- Gorodetskaya, I., N. van Lipzig, M. van den Broeke, W. Boot, C. Reijmeer, A. Mangold, S. Kneifel, S. Crewell, and J. Schween, Meteorological and cloud measurements at the Princess Elisabeth Belgian Antarctic Research Station, Dronning Maud Land, paper presented at the 5th Antarctic Meteorological Observation, Modeling and Forecasting Workshop, Byrd Polar Res. Cent., Ohio State Univ., Columbus, Ohio, 12 – 14 July, 2010.
- 325

- Gossart, A., Helsen, S., Lenaerts, J. T. M., Broucke, S. V., van Lipzig, N. P. M., & Souverijns, N.: An Evaluation of Surface Climatology in State-of-the-Art Reanalyses over the Antarctic Ice Sheet. *Journal of Climate*, 32(20), 6899–6915, <https://doi.org/10.1175/JCLI-D-19-0030.1>, 2019.
- 330 Gossart, Alexandra, Palm, S. P., Souverijns, N., Lenaerts, J. T. M., Gorodetskaya, I. V., Lhermitte, S., & van Lipzig, N. P. M.: Blowing snow in East Antarctica: comparison of ground-based and space-borne retrievals. *The Cryosphere Discussions*, 1–19, <https://doi.org/10.5194/tc-2019-25>, 2019.
- Hammer, C., Ohrnberger, M., & Schlindwein, V.: Pattern of cryospheric seismic events observed at Ekström Ice Shelf, Antarctica. *Geophysical Research Letters*, 42(10), 3936–3943, <https://doi.org/10.1002/2015GL064029>, 2015.
- 335 Herenz, P., Wex, H., Mangold, A., Laffineur, Q., Gorodetskaya, I. V., Fleming, Z. L., et al.: CCN measurements at the Princess Elisabeth Antarctica research station during three austral summers. *Atmospheric Chemistry and Physics*, 19(1), 275–294, <https://doi.org/10.5194/acp-19-275-2019>, 2019
- Hillers, G., Ben-Zion, Y., Campillo, M., & Zigone, D.: Seasonal variations of seismic velocities in the San Jacinto fault area observed with ambient seismic noise. *Geophysical Journal International*, 202(2), 920–932, <https://doi.org/10.1093/gji/ggv151>, 2015.
- 340 Johnson, C. W., Meng, H., Vernon, F., & Ben-Zion, Y.: Characteristics of Ground Motion Generated by Wind Interaction With Trees, Structures, and Other Surface Obstacles. *Journal of Geophysical Research: Solid Earth*, 2018JB017151, <https://doi.org/10.1029/2018JB017151>, 2019.
- Kojima S., & Shiraishi K.: Note on the geology of the western part of the Soer Rondane Mountains, East Antarctica, 43, 116–131, 1986.
- 345 Lepore, S., Markowicz, K. & Grad, M.: Impact of wind on ambient noise recorded by seismic array in northern Poland, *Geophysical Journal International*, Volume 205, Issue 3, Pages 1406–1413, <https://doi.org/10.1093/gji/ggw093>, 2016
- Lipovsky, B. P., & Dunham, E. M.: Tremor during ice stream stick-slip. *The Cryosphere Discussions*, 9(5), 5253–5289, <https://doi.org/10.5194/tcd-9-5253-2015>, 2015.

- 350 Lombardi, D., Gorodetskaya, I., Barruol, G., & Camelbeeck, T.: Thermally induced icequakes detected on blue ice areas of the East Antarctic ice sheet. *Annals of Glaciology*, 1–12, <https://doi.org/10.1017/aog.2019.26>, 2019.
- Lott, F. F., Ritter, J. R. R., Al-Qaryouti, M., & Corsmeier, U.: On the Analysis of Wind-Induced Noise in Seismological Recordings: Approaches to Present Wind-Induced Noise as a Function of Wind Speed and Wind Direction. *Pure and Applied Geophysics*, 174(3), 1453–1470, <https://doi.org/10.1007/s00024-017-1477-2>, 2017.
- 355 Matsuoka, K., Anders, S., & Deschwandan, A. V.: Quantarctica: A free GIS package for research, education, and operation in Antarctica. *Norwegian Polar Institute Seminar*, 2013.
- McNamara, D. E.: Ambient Noise Levels in the Continental United States. *Bulletin of the Seismological Society of America*, 94(4), 1517–1527, <https://doi.org/10.1785/012003001>, 2004.
- Mohr, J. J., Reeh, N., & Madsen, S. N.: Three-dimensional glacial flow and surface elevation measured with radar 360 interferometry. *Nature*, 391(6664), 273–276, <https://doi.org/10.1038/34635>, 1998.
- Mouginot, J., Rignot, E., & Scheuchl, B.: Continent-Wide, Interferometric SAR Phase, Mapping of Antarctic Ice Velocity. *Geophysical Research Letters*, 46(16), 9710–9718, <https://doi.org/10.1029/2019GL083826>, 2019.
- Mucciarelli, M., Gallipoli, M. R., Di Giacomo, D., Di Nota, F., & Nino, E.: The influence of wind on measurements of seismic noise. *Geophysical Journal International*, 161(2), 303–308, <https://doi.org/10.1111/j.1365-246X.2004.02561.x>, 2005.
- 365 Naderyan, V., Hickey, C. J., & Raspet, R.: Wind-induced ground motion. *Journal of Geophysical Research: Solid Earth*, 121(2), 917–930, <https://doi.org/10.1002/2015JB012478>, 2016.
- Pattyn, F., Declair, H., & Huybrechts, P.: Glaciation of the central part of the Soer Rondane, Antarctica: glaciological evidence. In: Yoshida, Y. et al. (Eds): *Recent Progress in Antarctic Earth Science, Terrapub (Tokyo)*, 669–678, 370 1992.
- Pattyn, Frank: Antarctic subglacial conditions inferred from a hybrid ice sheet/ice stream model. *Earth and Planetary Science Letters*, 295(3–4), 451–461, <https://doi.org/10.1016/j.epsl.2010.04.025>, 2010.
- Pattyn, Frank, Matsuoka, K., & Berte, J.: Glacio-meteorological conditions in the vicinity of the Belgian Princess Elisabeth Station, Antarctica. *Antarctic Science*, 22(01), 79, <https://doi.org/10.1017/S0954102009990344>, 2010.

- 375 Paul Winberry, J., Anandakrishnan, S., Wiens, D. A., & Alley, R. B.: Nucleation and seismic tremor associated with the
glacial earthquakes of Whillans Ice Stream, Antarctica: GLACIAL SEISMIC TREMOR. *Geophysical Research
Letters*, 40(2), 312–315, <https://doi.org/10.1002/grl.50130>, 2013.
- Peeters, K., Ertz, D., & Willems, A.: Culturable bacterial diversity at the Princess Elisabeth Station (Utsteinen, Sør Rondane
Mountains, East Antarctica) harbours many new taxa. *Systematic and Applied Microbiology*, 34(5), 360–367,
380 <https://doi.org/10.1016/j.syapm.2011.02.002>, 2013.
- Peterson, J.: *Observations and modeling of seismic background noise* (Open-File Report), 1993.
- Podolskiy, E. A., & Walter, F.: Cryoseismology: CRYOSEISMOLOGY. *Reviews of Geophysics*, 54(4), 708–758,
<https://doi.org/10.1002/2016RG000526>, 2016.
- Pushkareva, E., Pessi, I. S., Namsaraev, Z., Mano, M.-J., Elster, J., & Wilmotte, A.: Cyanobacteria inhabiting biological soil
385 crusts of a polar desert: Sør Rondane Mountains, Antarctica. *Systematic and Applied Microbiology*, 41(4), 363–373,
<https://doi.org/10.1016/j.syapm.2018.01.006>, 2018.
- Rignot, E., Mouginot, J., & Scheuchl, B.: Ice Flow of the Antarctic Ice Sheet. *Science*, 333(6048), 1427–1430,
<https://doi.org/10.1126/science.1208336>, 2011.
- Smith, A. M.: Basal conditions on Rutford Ice Stream, West Antarctica, from seismic observations. *Journal of Geophysical
390 Research: Solid Earth*, 102(B1), 543–552, <https://doi.org/10.1029/96JB02933>, 1997.
- Smith, A. M.: Microearthquakes and subglacial conditions. *Geophysical Research Letters*, 33(24), L24501,
<https://doi.org/10.1029/2006GL028207>, 2006.
- Souvereinjs, N., Gossart, A., Gorodetskaya, I. V., Lhermitte, S., Mangold, A., Laffineur, Q., et al.: How does the ice sheet
surface mass balance relate to snowfall? Insights from a ground-based precipitation radar in East Antarctica. *The
395 Cryosphere*, 12(6), 1987–2003, <https://doi.org/10.5194/tc-12-1987-2018>, 2018
- Stammler, K., & Ceranna, L.: Influence of Wind Turbines on Seismic Records of the Gräfenberg Array. *Seismological
Research Letters*, 87(5), 1075–1081, <https://doi.org/10.1785/0220160049>, 2016.

- Walker, K. T., & Hedlin, M. A. H.: A Review of Wind-Noise Reduction Methodologies. In A. Le Pichon, E. Blanc, & A. Hauchecorne (Eds.), *Infrasound Monitoring for Atmospheric Studies* (pp. 141–182). Dordrecht: Springer Netherlands, https://doi.org/10.1007/978-1-4020-9508-5_5, 2010.
- 400
- Winter, K., Lombardi, D., Diaz-Moreno, A., Bainbridge, R.; Monitoring Icequakes in East Antarctica with the Raspberry Shake. *Seismological Research Letters*; doi: <https://doi.org/10.1785/0220200483>, 2021.
- Withers, M. M., Aster, R. C., Young, C. J., & Chael, E. P.: High-Frequency Analysis of Seismic Background Noise as a Function of Wind Speed and Shallow Depth, 9, 1996.

405